

# Formation of granular jets

Dongyun He<sup>1</sup>, Prasad Ranganath Sonar<sup>1</sup>, Pradipto<sup>1</sup>, Kazuya U. Kobayashi<sup>2</sup>, and Yoshiyuki Tagawa<sup>1,\*</sup>

<sup>1</sup>Department of Mechanical Systems Engineering, Tokyo University of Agriculture and Technology, 2-24-16 Nakacho, Koganei-city, Tokyo, Japan

<sup>2</sup>Department of Mechanical Engineering, Nippon Institute of Technology, 4-1 Gakuendai, Miyashiro-machi, Minamisaitama-gun, Saitama, Japan

**Abstract.** Based on discrete element method (DEM) simulations, this study investigates the formation of granular jets triggered by the sudden unloading of a compressed granular column. After unloading, a jet can be generated from a granular column with a meniscus-shaped free surface. The evolution of jet velocity can be divided into two stages: the acceleration stage and the gravity-governed stage. In the gravity-governed stage, a grain stream can exhibit different regimes, including dispersed atomized grains, a sharp tip, and an elongated root. The effects of the key physical properties of grains on the jet velocity in the early stage are investigated. We find that a higher Young's Modulus is beneficial for generating a granular jet. The sliding friction coefficient and the coefficient of restitution have limited effects, which implies that the jet velocity is insensitive to the damping and tangential forces of the grains. Mass density significantly influences the velocity of granular jets. It is found that the jet velocity is proportional to the natural frequency of the grain-spring system. An increase in cohesion energy density leads to a reduction in jet velocity.

**Keywords:** Granular jet, Compression, Unloading, DEM simulation

## 1 Introduction

In liquid systems, focused jets can be generated using Pokrovski's experimental method, which releases a test tube partially filled with liquid to impact a rigid substrate. Antkowiak *et al.* [1] adapted liquid jet formation techniques to granular materials and demonstrated that meniscus-shaped free surfaces in granular piles can produce a focused jet, closely resembling the dynamics of liquid jets. This approach's simplicity presents opportunities for advancing the development of powder injectors in the medical field [2], optimizing spray dryers in the food industrial [3], and enhancing seed spraying applications in agriculture [4]. Regarding the focused granular jets, Antkowiak *et al.* [1] proposed that in both liquid and granular systems, the appearance of meniscus or concave shape of the free surface is a key to generating focused jets by using Pokrovski's method, otherwise, if the free surface is flat, a jet can not be formed. However, they did not delve into the factors that affect the formation of granular jets. Kobayashi *et al.* [5] investigated the effects of impact velocity and length of the grain column on the velocity of the granular jet and pointed out the crucial role of the impact velocity (shock strength) and the granular column length on the jet velocity. The results of their study align well with previous studies on interfacial instability, which proposed that the evolutions of the free surface strongly depend on the shock strength and the length of the granular columns [6, 7].

The above studies explained the effects of macroscopic initial parameters, *i.e.* the impact velocity and the column length of the granular pile, on the jet velocity. However, studies related to the effects of the physical parameters of a single grain on the jet formation are missing, although the physical properties of the grain itself can significantly affect the behaviors of granular flows [8]. Moreover, due to the opaque granular materials, it is hard to capture the de-

tails inside the jets experimentally. Therefore, simulations are required to see the full picture of a jet formation. In this research, the details of the granular jet formation and the effects of key physical parameters of mono-dispersed spherical grains (*i.e.* Young's Modulus, coefficient of restitution, friction coefficient, mass density, and cohesion energy density) on the average jet velocity are investigated.

## 2 Simulation methods

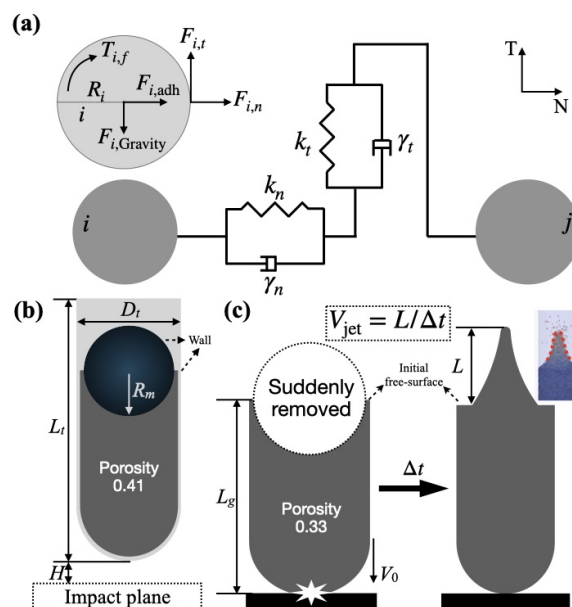


**Figure 1.** (a) a schematic showing two contacting grains *i* and *j*. The top-left inset details all forces acting on grain *i*. (b) the initial condition in the simulations before the unloading and impact. Details are listed in table 1. (c) an illustration of the jet velocity measurement.

\*e-mail: tagawayo@cc.tuat.ac.jp

## 2.1 Contact model

In this study, an open-source DEM solver, LIGGGHTS [9] is used to perform the simulations. All the forces and torques on a single grain are shown in figure 1(a). The Hookean model is used to calculate  $F_{i,n} = (k_n \delta \mathbf{n}_{ij} - \gamma_n \mathbf{v}_n)$  and  $F_{i,t} = \min\{|k_t \Delta \mathbf{s}_t - \gamma_t \mathbf{v}_t|, \mu_s F_{i,n}\}$ .  $F_{i,adh} = k_{CED} A$  is governed by the simplified Johnson-Kendall-Roberts (S-JKR) model and  $T_{i,f} = -\mu_r k_n \delta \mathbf{e}_{ij} R_i$  is calculated using the constant directional torque (CDT) model. These three models above are all included in the LIGGGHTS package [9].  $k_n = E^* R^* [(\frac{16}{15})^4 \frac{m^* V^2}{(R^*)^3 E^*}]^{\frac{1}{5}}$ , where the first term has spring constant dimension and the second is a dimensionless factor depending on the ratio of inertial pressure to Young's Modulus.  $k_t = \frac{2}{7} k_n$ ,  $\gamma_n = \sqrt{\frac{4m^* k_n}{1 + (\frac{m^*}{E^*})^2}}$  and  $\gamma_t = \gamma_n$  are the normal and tangential spring and damping coefficients, respectively.  $\delta$  is the overlap distance while grains contact in the normal direction,  $\mathbf{n}_{ij}$  is the unit vector along the center line of grain  $i$  and  $j$ .  $\mathbf{v}_n$  and  $\mathbf{v}_t$  are the normal and tangential components of relative velocity, respectively.  $\Delta \mathbf{s}_t$  is the tangential displacement vector.  $\mu_s$  and  $\mu_r$  are the sliding and rolling friction coefficients, respectively.  $R^*$ ,  $m^*$  and  $E^*$  are equivalent radius, mass, and Young's Modulus, respectively, where  $R^* = (R_i R_j)/(R_i + R_j)$ ,  $m^* = (m_i m_j)/(m_i + m_j)$  and  $E^* = [(1 - \nu_i^2)/(E_i) + (1 - \nu_j^2)/(E_j)]^{-1}$  where  $R_i$ ,  $m_i = (4/3)\pi R_i^3 \rho_i$  and  $\nu_i$  are the radius, mass and Poisson's ratio of grain  $i$  respectively, and  $\rho_i$  is the mass density.  $V$  is the characteristic impact velocity, one of the parameters used to calculate  $k_n$ .  $e$  is the coefficient of restitution.  $k_{CED}$  is the cohesion energy density in  $J/m^3$ .  $A = 4\pi R \delta$  is the contact area of grain  $i$  with  $j$ , and  $\mathbf{e}_{ij}$  is the relative direction of rotation between grain  $i$  and  $j$ .  $F_{i,Gravity} = m_i \mathbf{g}$  is the gravity of the grain  $i$  and  $\mathbf{g} = 9.8 \text{ m/s}^2$  is the gravitational acceleration.

## 2.2 Simulation setup and process

A DEM model consisting of a tube-shaped meshed boundary wall and monodisperse spherical grains is created, as shown in figure 1(b). The geometric parameters of the simulation system are listed in the table 1. Grains are generated from the top of the tube-shaped boundary at a constant rate until the number of grains reaches 75,000, while the grains accumulate at the bottom of the tube due to gravity. Since jet formation requires a meniscus-shaped free surface, once the system stabilizes, a spherical boundary moves uniformly along the negative direction of the z-axis, compressing the free surface. This reshaping process continues until the free surface closely approximates a hemispherical concave. After running the simulation to ensure the system reaches equilibrium again, the grains and tube-shaped boundary are set to move with uniform acceleration under the effect of gravity until they fall a distance  $H$ , at which unloading and impact occur. At the moment when the tube velocity reaches  $V_0 = \sqrt{2gH}$ , the tube-shaped wall is abruptly stopped, and the spherical boundary is instantly removed. This sudden unloading and impact initiate the formation of a granular jet. During motion, the spherical boundary responsible for reshaping the initial free surface moves at the same velocity as the grains, ensuring that the free surface shape is maintained. However, because the meshed ball compresses

**Table 1.** Geometric parameters in the simulations.

Item	Value	Definition
$D_g$	200 $\mu\text{m}$	Diameter of grain
$D_t$	8 mm	Diameter of tube
$R_m$	3.9 mm	Meniscus radius of free surface
$L_t$	60 mm	Diameter of tube
$L_g$	9 mm	Length of granular pile
$H$	20 mm	Distance of free falling

the granular column, significant residual forces among the grains are introduced, which dominate the jet formation. In this study, we focus on the formation of a granular jet driven by suddenly releasing the residual forces, hereafter the unloading-induced jet. Details regarding the impact-induced granular jet and the unloading-induced jet can be found in the Supplementary Material (SM).

The strategy of jet velocity measurement is illustrated in the figure 1(c). The average jet velocity is defined as  $V_{jet} = L/\Delta t$ , where  $\Delta t$  is the time interval after unloading and impact.  $L$  is the distance between the initial free surface and the tip of the jet after  $\Delta t$ . Due to the instability of granular flow, a dilute flow may be formed [10]. In this study, the tip of the granular jet marked by a red dashed curve is detected by a density-based spatial clustering of applications with noise (DBSCAN) algorithm proposed by Ester *et al.* [11]. At each time step, this algorithm is executed prior to measuring the jet velocity.

## 3 Results and discussions

### 3.1 The profile of the granular jet generation

In this section, the profile of the jet generation is investigated using different values of Young's Modulus  $E$  of grains and characteristic velocity  $V$  of the contact model mentioned in section 2.1. The details of the initial setting and important parameters used in the simulation are listed in the table 1 and 2, respectively.

As shown in figure 2(a), in the case of  $E = 100 \text{ MPa}$ ,  $V = 0.62 \text{ m/s}$  ( $k_n = 552.8 \text{ N/m}$ ), after unloading, the concave free surface gathers and disappears around 0.75 ms. Around 1.5 ms, the grains are aggregated into a string along the z-axis, and the jet begins to form. The shape of the jet evolves with time. At around 25 ms, three different regimes of the granular stream can be observed: I. dispersed atomized grains, II. sharp tip and III. elongated root. The dispersed atomized grains occur as the grains start to move, due to the instability of the free surface. To explain the formation of regimes of II and III, we assume that once the meshed ball is removed, the compressed granular column behaves like a spring composed of grains, instantly releasing its stored energy to eject the grains. The layer-by-layer release of grains from top to bottom due to the unloading results in a velocity gradient along the z-direction, which gives rise to an enlarged root. As shown in Figure S3, the residual force is greatest near the axis of symmetry of the granular pile. As a result, upon sudden unloading, grains in this region have the highest acceleration. In addition, due to the meniscus-shaped free surface, grains converge toward the center, leading to the formation of a sharp tip. For the case of  $E = 630 \text{ MPa}$ ,

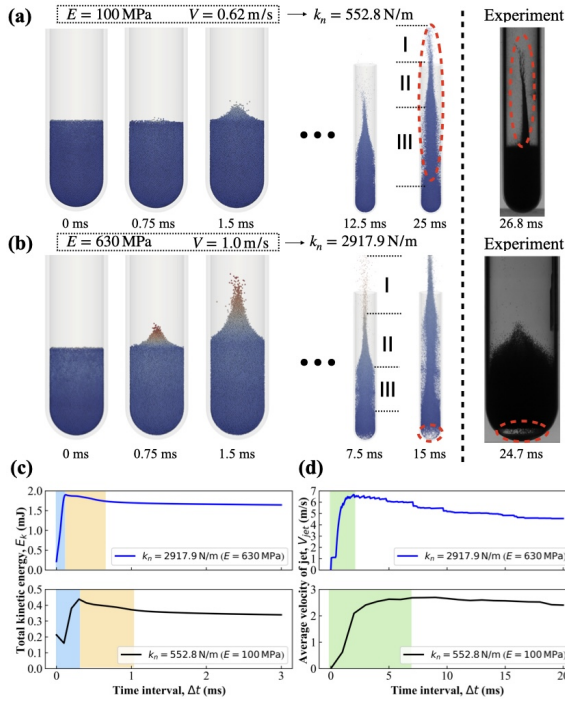


**Figure 2.** (a) and (b) are the temporal evolution of the granular jet formation after unloading and impact as  $E = 100$  MPa,  $V = 0.62$  m/s and  $E = 630$  MPa,  $V = 1$  m/s, respectively, and comparisons with experiments which the diameter of glass beads  $D_g = 45 \mu\text{m}$ ,  $D_t = 10.6$  mm,  $R_m = 5$  mm,  $L_g = 20$  mm, and  $H = 20$  mm for (a) and  $D_g = 215 \mu\text{m}$ ,  $D_t = 27.6$  mm,  $R_m = 13.2$  mm,  $L_g = 20$  mm, and  $H = 40$  mm for (b).

$V = 1$  m/s ( $k_n = 2917.9$  N/m) shown in figure 2(b), the evolution of the jet is faster than that in the former case.

To understand the effects of Young's Modulus on the jet formation, the evolutions of grains' kinetic energy  $E_k = \sum_{i=1}^N (1/2)m_i v_i^2$  is calculated, where  $v_i$  and  $N$  are the velocity of grain  $i$  and number of grains, respectively. After unloading, the potential energy stored in the granular pile is rapidly converted into the kinetic energy of the grains. As shown in figure 2(c), the kinetic energy increases almost instantaneously and peaks in a very short range, around 0.12 ~ 0.3 ms (highlighted with blue backgrounds). A steep drop in kinetic energy follows the peak, lasting about 0.48 ~ 0.95 ms (highlighted with yellow backgrounds), which may result from frequent collisions among densely packed grains during the initial phase of jet formation. Then, the kinetic energy decreases slowly. As shown in figure 2(d), the evolution of the average velocity of the jet can be roughly divided into two stages: the acceleration stage (marked in green) and the gravity-governed stage when the velocity decreases uniformly. A larger Young's Modulus of grains is beneficial for the forming of a granular jet because, at the same deformation level, a higher Young's Modulus leads to more stored potential energy in the granular pile, enabling grains to acquire more kinetic energy upon unloading.

Additionally, for different Young's Modulus, the two types of granular jets observed in the experiment are reproduced qualitatively in the DEM simulations. One is that the granular jet is formed from the dense granular base, which is marked by the red dashed lines in the fig-

**Table 2.** Parameters used in the DEM simulations

Parameter	Definition	Unit	Value
$\nu$	Poisson's ratio	-	0.24
$e$	Coefficient of restitution	-	0.7
$\rho$	Mass density	kg/m <sup>3</sup>	2500
$\mu_s$	Sliding friction factor	-	0.5
$\mu_r$	Rolling friction factor	-	0.01
$k_{CED}$	Cohesion energy density	kJ/m <sup>3</sup>	0

ure 2(a). The other one is that during the jet elongating, a cavity occurs at the bottom, which is marked in figure 2(b). Such similarities suggest that a compression-release process may also be involved in the formation of impact-induced granular jets.

### 3.2 Effects of key physical parameters on jet velocity in early regime

In this section, the effects of the physical parameters of grains on the average velocity of the jet in the early stage are investigated. Based on the values in the table 2, coefficient of sliding friction  $\mu_s$  (0.1 - 0.9), coefficient of restitution  $e$  (0.1 - 0.9), cohesion energy density  $k_{CED}$  (0 - 500 kJ/m<sup>3</sup>) and mass density  $\rho$  (500 - 8500 kg/m<sup>3</sup>), are varied separately in each simulation. As shown in figure 2(d), the average velocity of a jet reaches the maximum value before 10 ms when it is early stage for the jet formation. Therefore, this maximum value is chosen to characterize the velocity of a granular jet in the early regime.

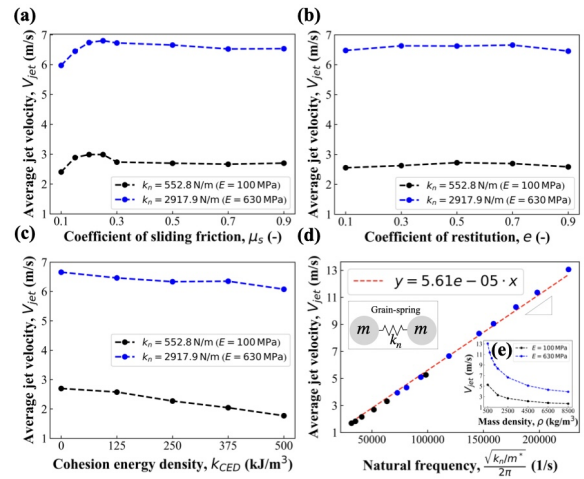


**Figure 3.** Effects of physical parameters of grain on the average velocity of the granular jet in the early stage.

In figure 3(a), with the increasing  $\mu_s$ , the velocity first increases then tends to remain constant, which may imply the occurrence of the sliding friction coefficient threshold below which may affect the jet behavior. As discussed in 2.1,  $\mu_s$  is related to the maximum value of  $F_{i,t}$ , which means that when the  $\mu_s$  is small, the value calculated by the deformation of grains can easily exceed this maximum value causing the value of  $F_{i,t}$  equal to the sliding friction. In this range, the increase of  $\mu_s$  leads to a larger  $F_{i,t}$ , which may benefit the formation of the jet. When the  $\mu_s$  is large enough and the value calculated by the deformation

of grains can not exceed the sliding friction, the  $F_{i,t}$  does not change with the  $\mu_s$ , leading to a constant jet velocity. For the coefficient of restitution  $e$  in figure 3(b), although a lower  $e$  leads to more energy dissipation, the jet velocity is not affected much. According to figure 3(c), the velocity is decreased by the increasing  $k_{CED}$ , which means that the cohesion may hinder the jet formation. As shown in figure 3(e), the velocity of the jet obviously decreases with the increasing mass density. To explain this trend, we simplify the system as a mass-spring model, in which a compressed spring with stiffness equal to the grain's normal stiffness  $k_n$  is used to launch a grain with mass  $m^*$ . The natural frequency of the simplified system is  $\frac{\sqrt{k_n/m^*}}{2\pi}$ . In figure 3(d), the horizontal axis is treated as natural frequency, and the linear trend implies that:

$$V_{jet} = \beta \sqrt{\frac{k_n}{m^*}} \quad (1)$$

where  $\beta$  is a fitting parameter with units of length, which may relate to the grain size or characteristic length. The increase in natural frequency enhances the responsiveness of grains to force variations. As a result, after unloading, grains begin to move more quickly in a system with a higher natural frequency, producing a higher jet velocity.

Overall,  $e$  and  $\mu_s$  have little effect on the jet velocity for the unloading-induced jets, while  $\rho$  has a significant impact. As discussed in 2.1,  $\mu_s$  is related to the tangential force ( $F_{i,t}$ ), and  $e$  is related to the damping coefficient ( $\gamma_n$  and  $\gamma_t$ ). It implies that the velocity of the granular jet is insensitive to changes in tangential force and damping coefficient. The jet velocity is linearly proportional to the natural frequency of the relevant mass-spring system.

## 4 Conclusions

After a granular jet is formed by unloading a compressed granular pile suddenly, the jet is first accelerated and then governed by gravity. Due to the instability of granular flow and velocity gradient along the z-axis, the jet evolves into three regimes: dispersed atomized grains, sharp tip, and elongated root. The normal force exerted on the grains due to the compression significantly influences the jet velocity, and the tube-shaped wall restricts the effects of tangential force. The dumping force and friction have limited effects due to the short contact time between grains when it flows rapidly. The increase in cohesive energy density enhances the tendency of grains to aggregate together, which in turn decreases the jet velocity. Mass density has significant effects on the velocity of granular jets. It has been found that the jet velocity is proportional to the natural frequency of the mass-spring system. However, how the grain size or the characteristic length affects the jet velocity needs to be further investigated. The jet formation mechanisms in the unloading-induced and impact-induced cases appear to differ. Therefore, the influence of grain-scale physical parameters on jet formation in the impact-induced case should be further investigated.

Moreover, Li *et al.* [12] observed an interfacial instability phenomenon by pressure shock in fluid-particle coupling simulation that resembles the jets in this research. Their study emphasizes the importance of particle-gas in-

teractions, which may suggest that considering air resistance in our study could lead to interesting findings. In addition, for the experimental photos in the figure 2(a) and (b), the quality of focusing for the granular jets is varied with the changing of the ratio of the tube diameter to the grain size. The mechanism leading to this phenomenon needs to be further investigated.

In the end, we gratefully acknowledge Dr. Satoshi Takada and Mr. Kohei Yamagata of Tokyo University of Agriculture and Technology for their insightful discussions, which provided valuable inspiration for this study.

## References

- [1] Antkowiak A, Bremond N, Le Dizès S, Villermaux E. Short-term dynamics of a density interface following an impact. *J. Fluid Mech.* **577**, 241-250 (2007). <https://doi.org/10.1017/S0022112007005058>
- [2] Sloat BR, Tran HK, Cui Z. *Needle-Free Jet Injection for Vaccine Administration.* (Wiley, 2012) 324-335. <https://doi.org/10.1002/9781118345313.ch21>
- [3] Fröhlich JA, Raiber TV, Hinrichs J, Kohlus R. Nozzle zone agglomeration in spray dryers: Influence of total solid content on agglomerate properties. *Powder Technol.* **390**, 292-302 (2021). <https://doi.org/10.1016/j.powtec.2021.05.094>
- [4] Wang Y, He M, Yan Q, Zheng Z. DEM-CFD simulation and seed orientation evaluation of a self-suction wheat shooting device. *Powder Technol.* **427**, 118746 (2023). <https://doi.org/10.1016/j.powtec.2023.118746>
- [5] Kobayashi K, Sato Y, Saito K, Masuda K, Tagawa Y. The generation and dynamics of a granular jet induced by a sudden acceleration, *Jpn. J. Multiphase Flow*, **38**, 319–326 (2024). <https://doi.org/10.3811/jjmf.2024.016>
- [6] Han P, Xue K, Bai C. Explosively driven dynamic compaction of granular media. *Phys. Fluids*, **33**, 023309 (2021). <https://doi.org/10.1063/5.0035475>
- [7] Koneru RB, Rollin B, Durant B, Ouellet F, Balachandrar S. A numerical study of particle jetting in a dense particle bed driven by an air-blast. *Phys. Fluids*, **32**, 093301 (2020). <https://doi.org/10.1063/5.0015190>
- [8] Mishra BK, Murty CVR. On the determination of contact parameters for realistic DEM simulations of ball mills. *Powder Technol.* **115**, 290-297 (2001). [https://doi.org/10.1016/S0032-5910\(00\)00347-8](https://doi.org/10.1016/S0032-5910(00)00347-8)
- [9] Kloss C, Goniva C, Hager A, Amberger S, Pirker S. Models, algorithms and validation for opensource DEM and CFD-DEM. *Prog. Comput. Fluid Dyn.* **12**, 140-152 (2012). <https://doi.org/10.1504/PCFD.2012.047457>
- [10] Guo Y, Curtis JS. Discrete element method simulations for complex granular flows. *Annu. Rev. Fluid Mech.* **47**, 21-46 (2015). <https://doi.org/10.1146/annurev-fluid-010814-014644>
- [11] Ester M, Kriegel HP, Sander J, Xu X. A density-based algorithm for discovering clusters in large spatial databases with noise. *KDD* **96**, 34 (1996).
- [12] Li J, Xue K, Zeng J, Tian B, Guo X. Shock-induced interfacial instabilities of granular media. *J. Fluid Mech.* **930**, A22 (2021). <https://doi.org/10.1017/jfm.2021.912>